Separation and Purification Technology 386 (2026) 136477

Contents lists available at ScienceDirect

Separation and Purification Technology

journal homepage: www.elsevier.com/locate/seppur

Energy-efficient recovery of ammonium by flow-electrode capacitive deionization using graphene-activated carbons

Fahrudin Sidik [a,b], Jr-Lin Lin [a,*], Ya-Ju Juang [c], Guan-You Lin [c]

[a] Department of Environmental Engineering, Chung Yuan Christian University, Chung-Li, Taiwan, ROC
[b] Department of Civil Engineering, Chung Yuan Christian University, Chung-Li, Taiwan, ROC
[c] Department of Water Treatment Modules and Products Research, Division of Water Technology Research, Material and Chemical Research Laboratories, Industrial Technology Research Institute, Hsinchu, Taiwan, ROC

ARTICLE INFO

Editor: G. Chen

Keywords:
Ammonium recovery
Capacitive deionization
Activated carbon
Graphene

ABSTRACT

Recovery of low-concentration ammonium (NH_4^+) from the effluent of municipal wastewater plants remains challenging because most existing electrochemical processes are energy-intensive to concentrate on ammonium. Flow-electrode capacitive deionization (FCDI) with activated carbon (AC) electrode slurries have been developed to achieve effective ion adsorption, but the inefficient NH_4^+ accessibility into AC pores and low energy-efficient implementation suppress FCDI scalability. The aim of this study was to reach energy-efficient ammonium recovery by a tailor-made graphene/nano-sized AC FCDI system by improving ion mobility. Various AC powders (200–1800 nm) and graphene loadings (0.5–1.5 wt%) were conducted at 1.4 V and 10 mL/min in the FCDI to evaluate the most energy-efficient configuration of AC slurries for NH_4^+ recovery. The results have shown that AC_{200} exhibits the most efficient NH_4^+ recovery, featuring a ten-fold concentration within 7 h reaction. Meso- and macropores of AC_{200} facilitate NH_4^+ transport and adsorption. However, AC_{1800} with excessive micropores leads to limited diffusion regardless of its large surface area. Moreover, the incorporation of 1.5 wt% graphene with 10 % AC_{200} can further improve ion transfer, resulting in the increase in specific capacitance by 2.53-fold. Meanwhile, the maximum NH_4^+ adsorption rate reaches 3.25×10^{-3} mg/cm^2/min where it shows the highest 99.43 % charge efficiency and the lowest energy input at 1.87 kWh/kg-NH_4^+. In addition, energy-efficient NH_4^+ recovery from low-concentration wastewater by FCDI using graphene/nano-sized AC electrode is feasible for practical applications. It is concluded that the manipulation of FCDI with nano-sized AC at optimal graphene/AC ratio is critical to reach energy-efficient NH_4^+ recovery from municipal wastewater in circular economy applications.

1. Introduction

Ammonium (NH_4^+) contamination in the aquatic environment contributes to eutrophication, groundwater pollution, and aquatic toxicity, posing a serious environmental threat and highlighting the importance of sustainable nitrogen recovery approaches [1,2]. Simultaneously, the growing demand for treated water and sustainable nutrient recovery has driven municipal wastewater treatment plants (WWTPs) to transition from pollutant removal towards resource recovery [3]. Although conventional municipal WWTPs remove 80–90 % of ammonia, residual ammonia at around 20–40 mg-NH_4^+/L remains a valuable material for recycling. This recovered ammonia can be repurposed for the agricultural and industrial sectors, including textile manufacturing, water purification, precious metal extraction, and semiconductor wafer cleaning [4–7]. Therefore, efficient NH_4^+ recovery technologies are essential to mitigate environmental impacts and meet the increase in demand for NH_4^+ resources.

Various technologies, including physicochemical, biological, and electrochemical methods, have been applied for NH_4^+ recovery from wastewater. The most common methods, such as air stripping, struvite precipitation, ion exchange and membrane processes, are less effective and not beneficial for low-concentration wastewater (<100 mg/L) because of high energy demand, low selectivity, and complex operation [8–10]. Instead, electrochemical approaches, including bio-electrochemical systems (BES), can treat low-strength wastewater with relatively low energy input, but typically achieve limited NH_4^+ recovery rates (<40 g N m^{-2} d^{-1}) and may require aeration, which increases operational expenditure [11]. To date, traditional capacitive

* Corresponding author.
E-mail address: jrlin@cycu.edu.tw (J.-L. Lin).

https://doi.org/10.1016/j.seppur.2025.136477
Received 21 August 2025; Received in revised form 3 December 2025; Accepted 11 December 2025
Available online 12 December 2025

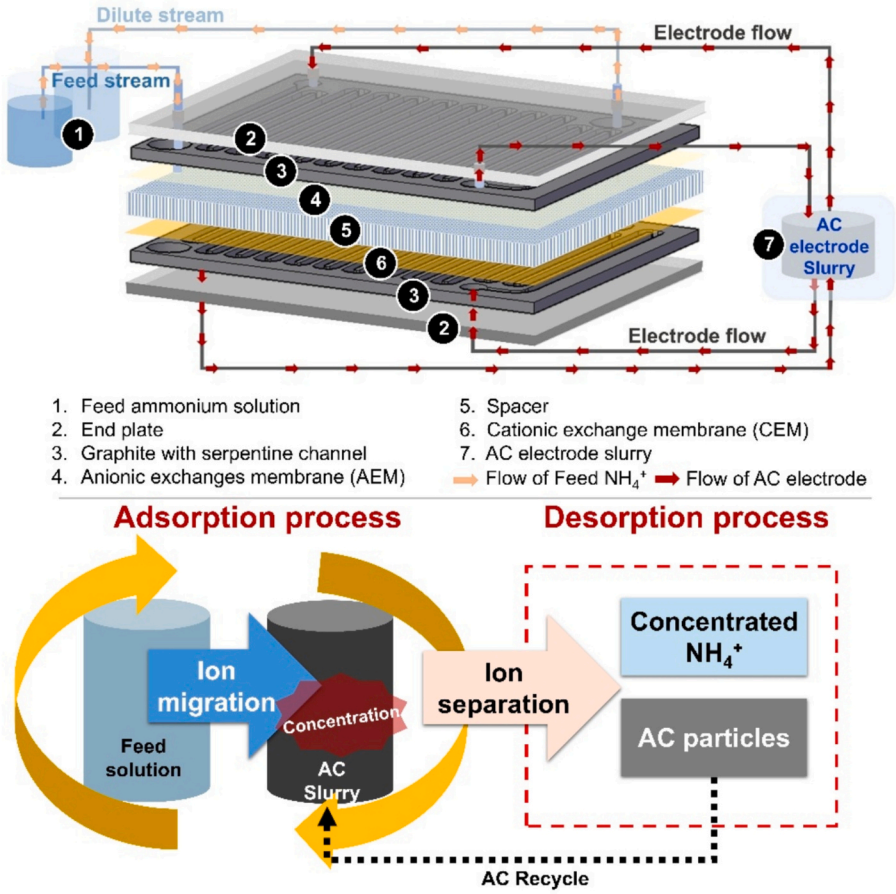

Fig. 1. Schematic diagram of the FCDI system operation.

deionization (CDI)-based technologies applied in wastewater treatment have been proven to achieve 77–96 % of NH_4^+ adsorption from 4 to 1000 mg-N/L and reach 38–82 % recovery rate of NH_4^+-N. However, the recovery of low-concentration NH_4^+ from effluent by traditional CDI typically pays off high energy input (7.8–38.5 kWh/kg-NH_4^+) but limited adsorption in its intermittent operation mode [12–15]. In contrast, flow-electrode capacitive demonization (FCDI) is an advanced CDI-based configuration that utilizes pumpable AC suspensions as electrodes, enabling pseudo-infinite adsorption through reloading electrode slurries in a continuous operation mode, which offers 87–90 % of NH_4^+ adsorption at initial 40 mg/L of NH_4^+ and lower energy demand in the range of 6 to 30 kWh/kg-NH_4^+ [16,17] at unlimited recovery of ammonium. Thus, FCDI is considered an applicable approach to reach energy-efficient NH_4^+ recovery from the effluent of municipal WWTPs.

Recently, extensive improvements on NH_4^+ adsorption by carbon-based FCDI system have been studied through material modification, reactor design, and tuning key parameters such as pH, flowrate, viscosity of slurry, and the addition of conductive materials to lower energy input ranging from 1.8 to 5 kWh/kg-NH_3 [17–22]. Previous studies have emphasized that modifications of electrode materials are able to effectively improve ammonium recovery with low energy input. Compared to unmodified AC, the sodium dodecyl sulfate- (SDS-AC) material could enhance ammonium adsorption capacity over 115 % with ~2.2 times lower energy input [23]. Mixed potassium ditianate ($K_2Ti_2O_5$ or KTO) with AC shows higher adsorption selectivity from 2.3 to 31 towards NH_4^+ over Na^+, with energy consumption of approximately 2.49 kWh/kg-N [19]. In fact, the application of carbon-based materials is the most practical approach because it has large specific surface area, high electrical conductivity, robust electrochemical stability, and cost-effectiveness [24]. However, the particle size distribution of micro-size AC slurries with and without fine AC (~400 nm) critically influences the adsorption kinetics of monovalent ions (e.g., Na^+), electron transport efficiency, and slurry stability [25], with maximum Na^+ adsorption at around 72 % due to excellent pore accessibility and charge transport. Nevertheless, a previous study has demonstrated that incorporating AC (diameter:5.6 μm; S_{BET}:1770 m^2/g) with graphite can enhance NH_4^+ recovery from 20 to 320 mg-N/L because the addition of graphite enables the accelerated ion adsorption–desorption kinetics and extended π–electron networks, while the energy input increases over reaction time within 7 h, reaching approximately 3.89 kWh/kg-N [26]. Although the individual effects of particle size on monovalent (Na^+ or NH_4^+) adsorption capacity and improvement in energy input have been examined independently for AC-based FCDI, the synergistic effect of nano-sized AC and graphene mixture on NH_4^+ adsorption and energy input is under investigation, especially at low-concentration of ammonium (<100 mg-NH_4^+/L).

The aim of this study was to investigate the diameter effect of nano-sized AC electrodes on NH_4^+ adsorption and energy consumption using FCDI with and without graphene. The physico-chemical characteristics, including morphology, specific surface area, pore volume and surface functional groups of various AC particles were determined to propose NH_4^+ adsorption mechanisms at different AC diameters without graphene. To study the synergistic effect on NH_4^+ adsorption and energy consumption with graphene incorporating with AC electrode, average adsorption ammonium rate, current efficiency, energy-normalized removed salt (ENRS) and specific energy consumption were determined at various graphene/AC ratios to evaluate the role of graphene in energy-efficient NH_4^+ recovery by FCDI.

2. Materials and methods

2.1. Materials and reagents

All chemicals used in this study were of analytical grade and procured from Sigma-Aldrich. Cation- and anion-exchange membranes were supplied by IONSEP (Lanran). All the solutions were prepared with Milli-Q water (resistivity: 18.2 MΩ cm). The ammonium feed solution was prepared by dissolving 5.54 mM of NH_4Cl in deionized water. A real wastewater sample was prepared through the collection of effluent from municipal WWTP, and the metal ions were quantified by inductively coupled plasma-optical emission spectrometry (ICP-OES, Shimadzu, Japan). To produce fine particles at different diameters, including 200 nm (AC_{200}), 600 nm (AC_{600}), and 1800 nm (AC_{1800}), the commercial AC (2-3 μm) was crushed by using a dry ball mill equipped with 20 mm and 5 mm balls, operated at 300 rpm for 3 h as illustrated in Fig. S1. AC particle size distributions were measured using a Zetasizer Nano ZS (Malvern, UK). Electrode AC slurries were prepared by mixing the desired amount of AC (7.5 and 10 wt%) in deionized water with and without addition of graphene ($GP_{0.5}$: 0.5 wt% and GP $_{1.5}$: 1.5 wt%) following previous studies [24,27,28], as shown in Table S1. Graphene exhibited stacked thin sheets with characteristic D and G bands at 1334 and 1580 cm^{-1}, and 2D-related peaks at 2467–2681 cm^{-1}, as confirmed by scanning electron microscopy (SEM; SM-7600F, Jeol, Japan) and raman spectroscopy (Fig. S2a and b). The morphology of AC before and after ball-milling was observed by SEM scanning, as shown in Fig. S2c–e. It proves that nano-sized AC particles were successfully prepared and uniformly dispersed along the graphene sheet-like structures after mixing. To enhance dispersion stability, AC was pretreated with HNO_3 to introduce oxygen-containing functional groups that improved hydrophilicity and provided anchoring sites for graphene. The mixtures of AC slurries were stirred for 24 h before testing to obtain a well-dispersed AC suspension and were subsequently fed into the FCDI cell during the experiments.

2.2. Protocol of FCDI manipulation

A schematic diagram of the FCDI process and the reactor is shown in Fig. 1. The FCDI reactor consisted of three compartments configured with a pair of graphite current collectors featuring serpentine flow channels with 2 mm depth and 2 mm width. A cation exchange membrane (CEM) and anion exchange membrane (AEM) were placed between the current collector and separated by PTFE mesh sheets (60 mm × 80 mm, ~0.5 mm thick) as spacers. The effective contact areas between the ion exchange membranes and serpentine flow channels were 29.6 cm^2. Silicone rubber gaskets with a thickness of 0.5 mm were used between compartments to prevent leakage. The endplates of the FCDI reactor were made of 2 cm thick acrylic material. A full configuration of the assembled FCDI reactor is shown in Fig. S3.

A short-circuited closed-cycle (SCC) mode was adopted to recirculate the AC slurry from the AC feed tank into the reactor at a constant flow rate of 10 mL/min using peristaltic pumps [29]. The SCC mode allows ions adsorbed in the electric double layers (EDLs) to be released by neutralization, maintaining the ionic charge balance and pH stability in the AC slurry [30]. In this study, the FCDI was conducted in constant voltage mode (1.4 V) using the chronoamperometry technique (Potentiostat SP-50e, BioLogic, France). The pH and conductivity of the ammonium feed solution were monitored in real time with a pH and conductivity multiparameter (Hach HQ411D, USA). The pH of the AC slurry electrode was measured using a pH meter, and the ammonium concentrations in both the feed solution and AC slurry were determined using an ammonia ion-selective electrode (ISE, Hanna Instruments H5222, Italy).

2.3. Analysis of AC slurry samples

To calculate the ammonium concentration, the collected AC slurry was first centrifuged at 6000 rpm for 15 min, and the ammonium-rich supernatant was measured. To determine the ammonium trapped on the AC particles, the pellets of the AC slurry were acidified with 0.1 N HCl and stirred for 10 min. The acidified mixture was then centrifuged at 6000 rpm for 15 min. The ammonium concentration in the supernatant was measured to determine the amount of ammonium adsorbed onto the AC particles.

2.4. Analysis of electrochemical characteristics

To evaluate the electrochemical characteristics of the AC electrode, cyclic voltammetry (CV) and electrochemical impedance spectroscopy (EIS) were conducted using a potentiostat (SP-50e, BioLogic, France) in a three-electrode system. The CV test was performed at −1 to 1 V vs the reference electrode at scan rates of 2, 10, and 20 mV/s, and 5 repetition in 1 M of NH_4Cl solution. The EIS test was performed at a low amplitude of 10 mV in the frequency range of 100 kHz–100 Hz. The obtained EIS data were fitted to Nyquist plots. The specific capacitance (C_s) was calculated using the following formula:

$$C_s\ (F/g) = \frac{\int ivdv}{2\mu m \Delta V} \tag{1}$$

where i is the current (A), v is the potential (V), μ is the scan rate (mV/s), m is the active mass of the electrode material (g), and ΔV is the potential window during testing.

2.5. Calculations and performance evaluations

The reduction ratio (%) of conductivity and ammonium, average ammonium adsorption rate (AAAR, mg-NH_4^+/cm^2·min), current efficiency (CE, %), energy-normalized removed salt (ENRS, μmol/j), and energy consumption (kWh/kg- NH_4^+) were calculated according to Eqs. (2)–(6), listed as below [26,31]:

$$Reduction\ ratio\ (\%) = \left(1 - \frac{C_t}{C_0}\right) \times 100 \tag{2}$$

where C_0 is the initial concentration (mg/L), C_t is the concentration at a certain time t (mg/L).

$$AAAR\left(mg_{NH_4^+} \Big/ cm^2 \bullet min\right) = \frac{V(C_0 - C_t)}{A_{eff} \times t} \tag{3}$$

where V is the volume of the sample, C_0 is the initial concentration (mg/L), C_t is the concentration at a certain time, A_{eff} is the effective area of the electrode to the membrane (29.6 cm^2), and t is the operational time.

$$CE\ (\%) = \frac{nFV(C_0 - C_t)}{M \int_0^t I\, dt} \times 100 \tag{4}$$

where n is the charge, F is the Faraday constant (96500), V is the volume of the sample, C_0 is the initial concentration (mg/L), C_t is the concentration at a certain time, M is the molar mass, and I is the current.

$$ENRS\left(\frac{\mu mol}{j}\right) = \frac{V\,(C_0 - C_t)}{\int_0^t IU\, dt} \tag{5}$$

where $V$is is the volume of the sample, C_0 is the initial concentration (mg/L), C_t is the concentration at a given time, I is the current, and U is the applied voltage (1.4 V).

$$Energy\ consumption\left(kWh \Big/ kg_{NH_4^+}\right) = \frac{\left(U \int_0^t I\,(t) dt\right) \times 2.7778 \times 10^{-7}}{V(C_0 - C_t) \times \eta} \tag{6}$$

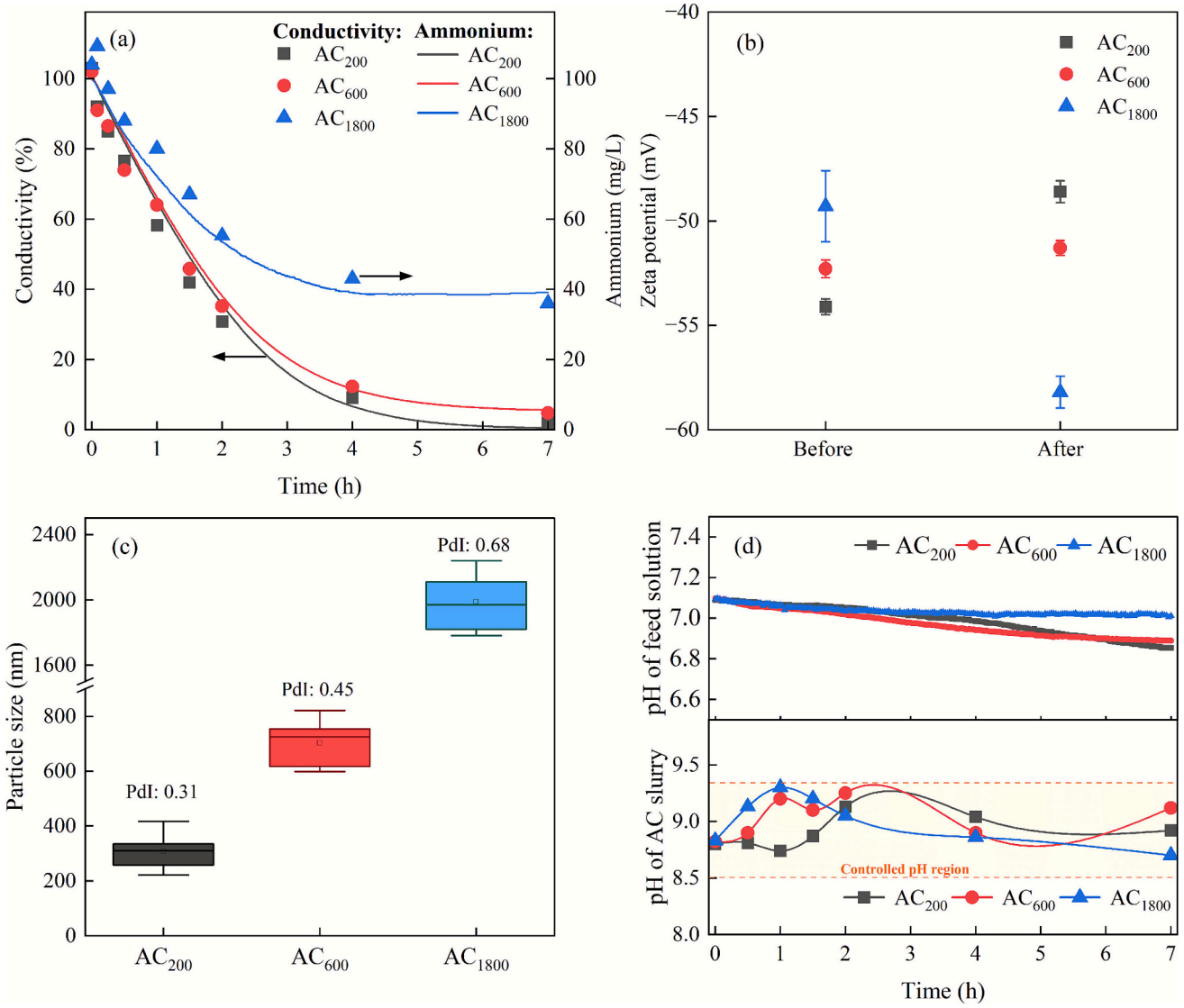

Fig. 2. Changes in (a) conductivity and ammonium concentration, (b) zeta potential, (c) particle size and the corresponding polydispersity index of particles (PdI), (d) pH feed solution and AC slurry at different AC particle sizes (AC_{200}: 200 nm, AC_{600}: 600 nm, AC_{1800}: 1800 nm) during 7 h operational time of FCDI operation at 1.4 V (initial pH of feed solution: 7 ± 0.2 and operating pH of AC slurry: 8.8 ± 0.2).

where U is the voltage, i is the current, t is the time, 2.7778×10^{-7} is the conversion factor of joule to kwh $\frac{1}{3.6\times10^{5}} = 2.7778 \times 10^{-7}$ kWh per joule), V is the volume of the sample, C_0 is the initial concentration (mg/L), C_t is the concentration at a certain time, and η is removal efficiency.

3. Results and discussion

3.1. Impact of AC electrode size on ammonium adsorption

The changes in conductivity and ammonium concentrations from the feed solution were studied to understand the impact of various AC diameters towards ammonium adsorption via FCDI under an applied voltage of 1.4 V for 7 h, as shown in Fig. 2a. AC_{200} exhibits the fastest conductivity reduction followed by AC_{600} with remaining ammonium concentrations of 1.95 mg/L and 4.7 mg/L, respectively. In contrast, AC_{1800} shows the lowest performance with a remaining ammonium concentration of ~40 mg/L. The superior ammonium adsorption by AC_{200} can be attributed to its favorable ionic transport behavior, as indicated by the AC surface charge variations (Fig. 2b). AC_{200} exhibits more markedly negative surface charges of approximately −54 mV before FCDI operation, leading to enhance NH_4^+ adsorption via electrostatic interactions. A stronger negative surface charge correlates with the occurrence of a high density of functional groups (—COO^-, -OH, C═O), which could facilitate ammonium adsorption [32]. A previous study has reported that the negative surface charge can result from the increase in repulsive forces among particles [33]. This phenomenon aligns with the lower polydispersity index of particles (PdI) value at AC_{200} (Fig. 2c), which indicates uniform and stable particle size distribution. Unlike larger AC electrodes, the pronounced negative surface charge and higher dispersity of smaller AC electrodes could cause more efficient NH_4^+ adsorption due to strong attraction between NH_4^+ and binding sites on AC surface. In addition, smaller AC electrodes could provide a high interconnectivity among AC particles, thereby accelerating NH_4^+ ion transfer to reach the AC surface [25]. Meanwhile, high dispersion stability of AC_{200} minimizes agglomeration and maintains flowability. In summary, when the size of AC electrodes reduces to nano size from micro size, the superior suspending ability of AC electrodes may induce frequent contacts between nano-sized suspended AC and NH_4^+ within the serpentine channel during FCDI, leading to faster ammonium adsorption. It is worth noting that the NH_4^+ adsorption increases insignificantly within 7 h FCDI operation, with less than 3 %, as

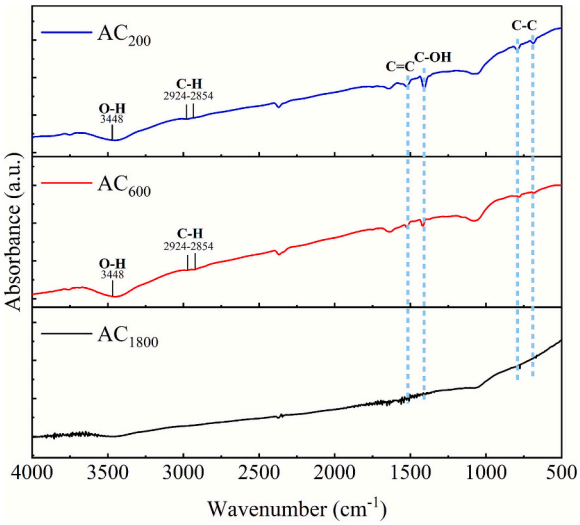

Fig. 3. FTIR spectra of AC slurry with different AC sizes (AC_{200}: 200 nm, AC_{600}: 600 nm and AC_{1800}: 1800 nm) after 7 h of FCDI operation at 1.4 V (initial pH of feed solution: 7 ± 0.2 and operating pH of AC slurry: 8.8 ± 0.2).

the size of AC reduces from 600 nm to 200 nm. These particle-size-dependent effects enhance ammonium accessibility towards the AC particle surface prior to intraparticle diffusion. This indicates that another influencing factor, such as pore properties of AC, could significantly dominate the ion adsorption aside from AC size effect. During the FCDI operation, pH of feed solution remained stable with only minor decreases to ~6.8 at AC_{200} and AC_{600} (Fig. 2d). This pH stability indicates that ammonium adsorption is not primarily governed by pH. Likewise, the pH of AC slurry was maintained within 8.6–9.3 in order to prevent conversion of NH_4^+ become NH_3 gas.

3.2. *Effect of physico-chemical characteristics of nanopore AC on ammonium recovery*

Although the size of AC electrodes mainly governs external ion transfer and stability of AC electrodes before internal adsorption by porous structure of AC electrodes, physico-chemical characteristics (i.e., binding site and pore fraction) would also substantially affect the adsorbed amount of ammonium from pure NH_4^+ solution [34]. In this study, chemical properties of AC particles at different sizes were further analyzed using FTIR spectroscopy to investigate the variations in the surface functional groups, as shown in Fig. 3. The broad absorption band at 3448 cm^{-1} corresponds to O—H stretching vibrations, indicating the presence of hydroxyl groups, which has likewise been attributed to O—H stretching in related electrochemical systems [35]. A weaker C—H stretching vibration representing characteristic of aliphatic hydrocarbon is observed within the 2924–2854 cm^{-1} range [36]. The presence of a stronger carbonyl stretching peak suggests the formation of surface-bound carbonyl groups, which is likely resulting from the acidic treatment during activation [37]. The FTIR spectrum of AC_{1800} exhibits limited peaks, indicating a minimum surface chemical activity, which could be attributed to a higher degree of graphitization or the absence of functional oxygen-containing groups. In contrast, AC_{600} displayed distinct peaks at 1540, 1415, and 805 cm^{-1}, corresponding to C═C (aromatic ring stretching), C—OH (hydroxyl groups), and C—C (skeletal

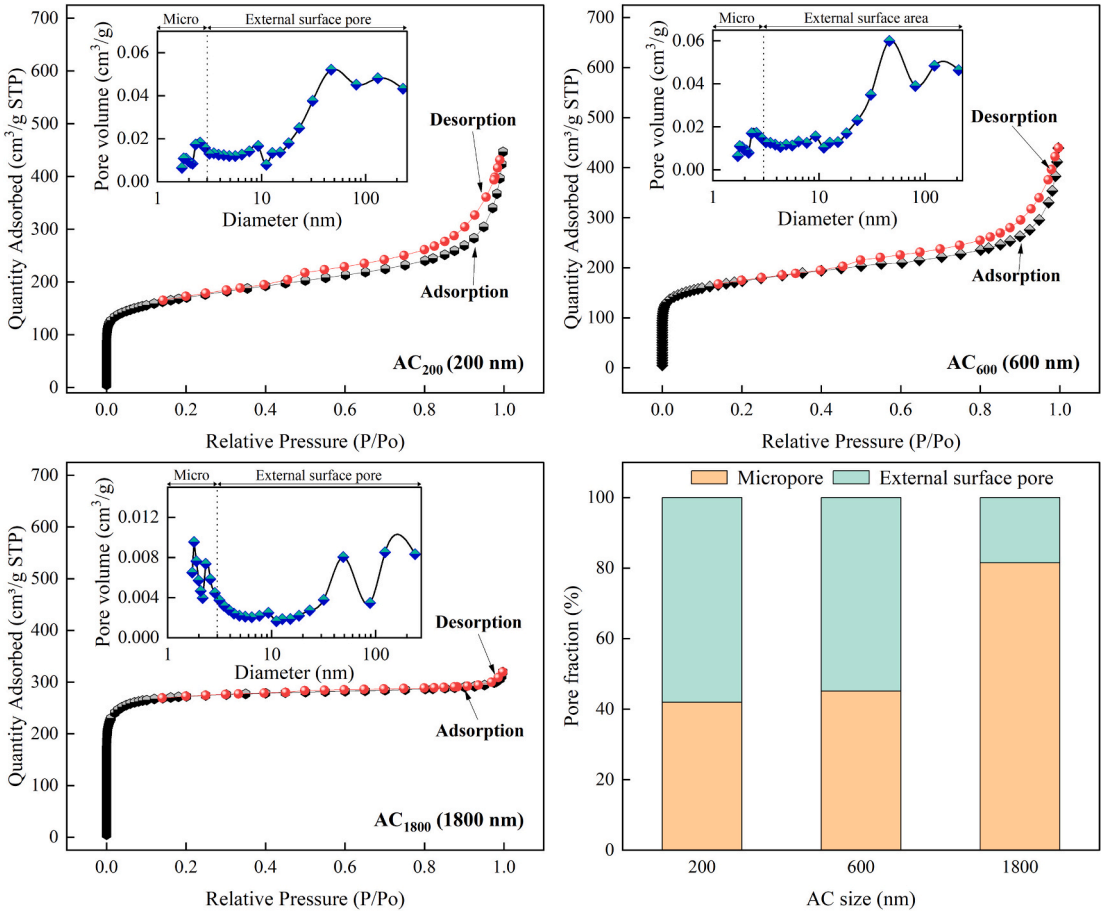

Fig. 4. Nitrogen adsorption and desorption isotherm, pore size distribution, and pore fraction of various AC particles sizes (200, 600, 1800 nm) based on the pore volume obtained from BET method

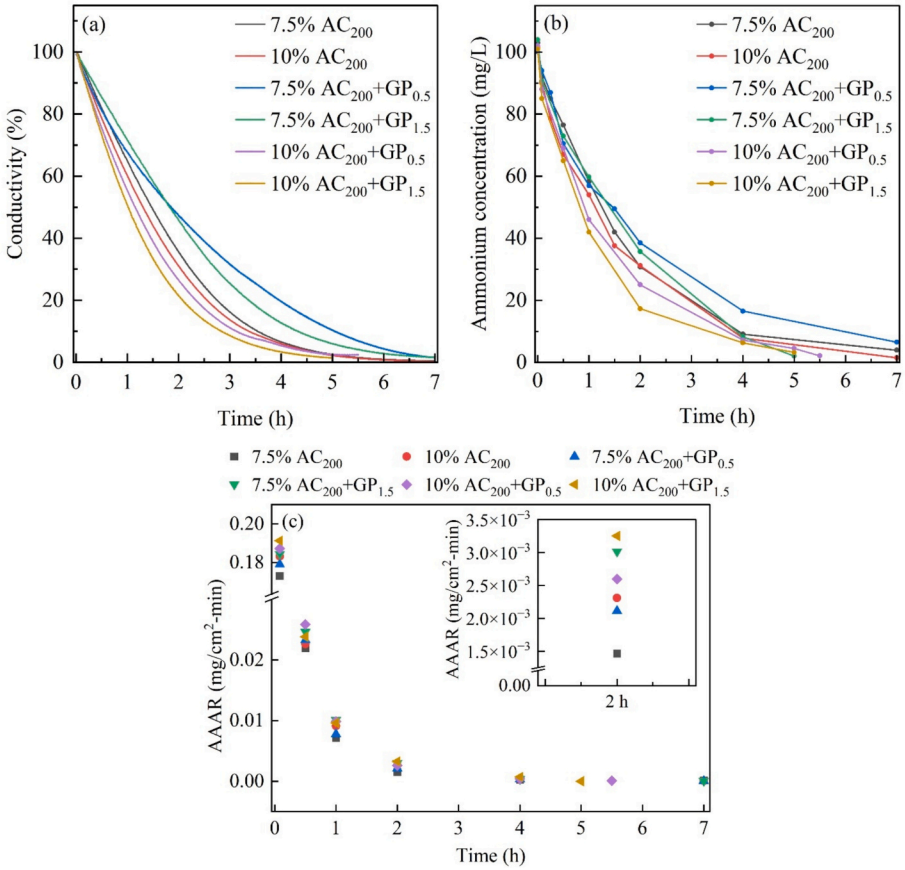

Fig. 5. Changes in (a) conductivity, (b) ammonium concentration, and (c) average ammonium adsorption rate (AAAR) at the different AC_{200} (200 nm) contents and the addition of graphene during 7 h of FCDI operation at 1.4 V (initial pH of feed solution: 7 ± 0.2 and operating pH of AC slurry: 8.8 ± 0.2).

vibrations), respectively. The absorption bands observed in the 1500–1600 cm^{-1} range could result from aromatic ring stretching coupled with carboxylate vibrations, as reported previously [38]. Notably, AC_{200} exhibits the most pronounced peaks, particularly for O—H, C—H, C-OH, and C—C functional groups that are favorable to increase chemical reactivity. It suggests that the abundant functional groups of AC_{200} behave strong surface hydrophilicity and charge-assisted NH_4^+ adsorption, which further complements the particle-size-driven impact on ammonium transfer.

The specific surface area and pore volume of AC electrode with varying AC particle diameters were analyzed to evaluate their impact on NH_4^+ adsorption onto AC electrode in the manipulation of FCDI, as shown in Fig. 4. The results indicate that AC_{1800} has the highest surface area, approximately 842.675 m^2/g, followed by AC_{200} and AC_{600} exhibiting approximately 560.4 m^2/g and 566.521 m^2/g, respectively. Based on the adsorption test on the surface area of AC, this predominant surface area in AC_{1800} is demonstrated by the adsorbed nitrogen gas into micropore structure. Such micropore-dominated structures in AC_{1800} inherently limit the accessibility and diffusion of hydrated NH_4^+ ions. However, the total pore volume of AC_{1800} micropore is only approximately 0.121 cm^3/g, which is fourfold lower compared to AC_{200} and AC_{600}, indicating that its internal pore spaces are less available for ion adsorption. At such conditions, predominated microporous AC can promote stronger ion-wall interactions, which causes limited ion diffusion and lower adsorption kinetics. A previous study has demonstrated that variations in pore size critically influence ion migration capacity and transport efficiency [31]. In contrast, both AC_{200} and AC_{600} in the FCDI system have a similarly high proportion of external surface pores composed of mesopores and macropores, which can enhance ion transport and reduce electric resistance. These wider pore channels reduce ion-wall interactions and facilitate bulk-like transport, allowing NH_4^+ to penetrate deeper into the carbon matrix. In other words, ion mobility is dictated by pore size distribution in which larger mesopores and macropores minimize ion-wall interactions to facilitate bulk-like transport and enhance adsorption efficiency. Therefore, the external pore volume can be significantly magnified as the size of AC electrodes reduces from micro to nano dimension, while it has limited increase in external pore volume as the nano-sized AC is diminished further to smaller one by which the insignificant NH_4^+ adsorption appears. This indicates that the effect of external pore size plays a dominant role in NH_4^+ adsorption after diminishing AC electrodes to nano dimension. In summary, smaller AC electrodes with dominant external surface area generated from mesopore and macropore facilitate ion transport to reach vast NH_4^+ adsorption, while larger AC electrodes with larger microporous surface areas contribute to slower ion transport that delay NH_4^+ adsorption.

3.3. Synergistic effects of graphene-AC electrode on ammonium recovery

Energy consumption remains a critical challenge in the application of FCDI for ammonium recovery. In this study, stand-alone AC electrodes still demonstrate an energy input exceeding 2 kWh/kg-NH_4^+, as shown in Fig. S4. With AC_{200} alone, it results in the lowest energy consumption at approximately 2.5 kWh/kg-NH_4^+, followed by AC_{600} and AC_{1800} accounting for 3.2 and 6 kWh/kg-NH_4^+, respectively. A previous study has revealed that graphene can improve electrical conductivity and assist the ion adsorption [39]. To further evaluate the effect of graphene incorporation with AC for ammonia recovery improvement, two graphene amounts of 0.5 and 1.5 wt% were mixed with AC slurry at 7.5 % and 10 wt%. As shown in Fig. 5a and b, it shows that the addition of 0.5

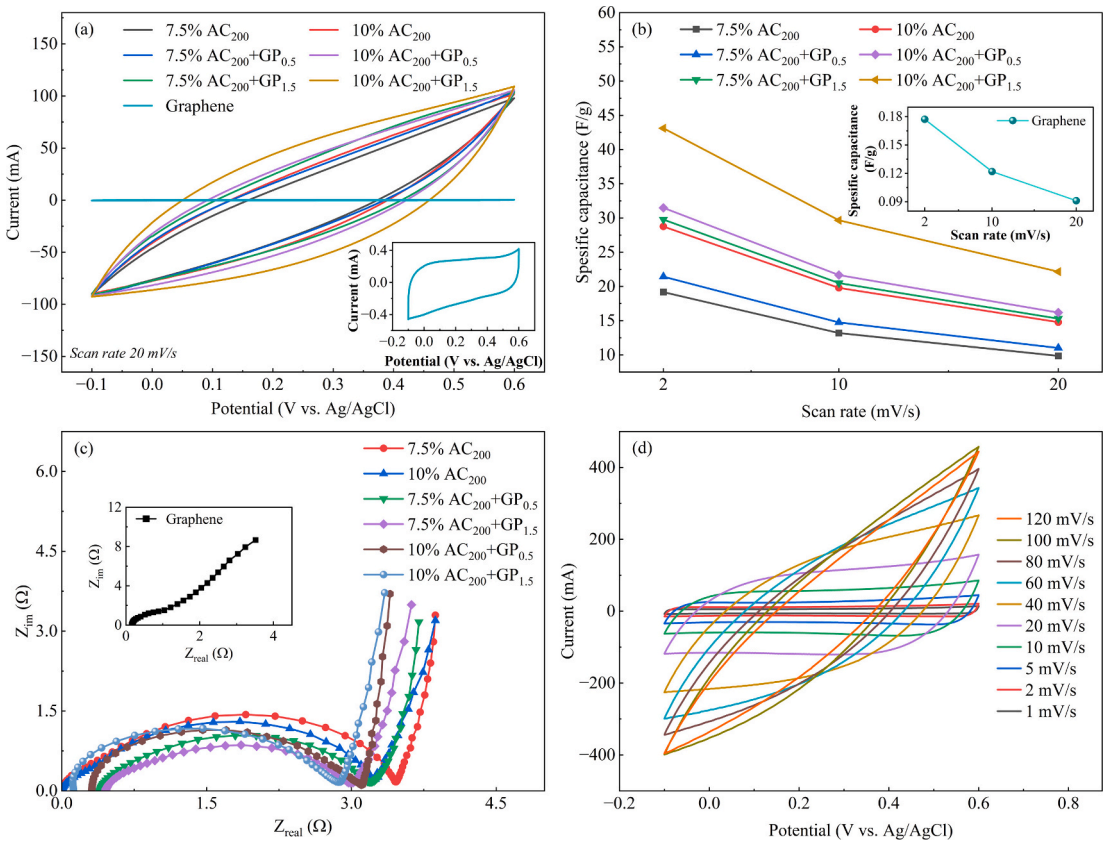

Fig. 6. Variation in (a) CV curves at a 20 mV/s scan rate, (b) specific capacitance of the AC slurry, (c) EIS represented by a Nyquist plot at the different AC_{200} (200 nm) contents and the addition of graphene, and (d) CV curves at varying scan rates in a 1 M NH_4Cl electrolyte

% and 1.5 % graphene into 7.5 wt% AC_{200} slurry initially reduces both conductivity and ammonium removal because the presence of graphene could occupy the partial binding site on the AC surface. A previous study has revealed that the incorporation of additive materials such as CNTs enhances electrical conductivity and restricts ion or charge transfer to adsorption sites [40].

Despite the incorporation of graphene with 7.5 wt% AC_{200} slurry slightly reduces the NH_4^+ adsorption onto the AC electrodes within first 2 h, as increasing AC_{200} amount to 10 wt%, it further improves NH_4^+ adsorption significantly. In that case, after 2 h of adsorption, with AC_{200} alone, it reaches 70 % of NH_4^+ adsorption, while 10 % AC_{200} mixed with 1.5 % graphene shows the most improvement in NH_4^+ adsorption up to 83 %. Therefore, 10 % AC_{200} and 1.5 % GP mixture possesses synergistic effect on NH_4^+ adsorption.

To further evaluate the effect of graphene on adsorption kinetics of NH_4^+ by FCDI at various graphene/AC ratio, the average ammonium adsorption rate (AAAR) was calculated using Eq. (3), as shown in Fig. 5c. With 7.5 % AC_{200} alone, it exhibits the lowest AAAR, accounting for 1.57×10^{-4} mg/cm^2/min within 2 h. However, with the addition of 0.5 and 1.5 wt% graphene can rise AAAR to 1.46×10^{-3} and 3.01×10^{-3} mg/cm^2/min, respectively. Likewise, increase in AC_{200} amount to 10 wt % achieves higher AAAR at 0.5 wt% graphene (10 % AC_{200} + $GP_{0.5}$) and 1.5 wt% graphene (AC_{200} + $GP_{1.5}$) at approximately 2.1×10^{-3} and 3.25×10^{-3} mg/cm^2/min, respectively. These results suggest that the addition of graphene into AC slurry improves charge transfer by providing additional conductive pathways, leading to reduce electrical resistance and facilitating ion migration towards the active adsorption sites [20,41]. In fact, the adsorption performance of graphene-AC could be declined in a multiple-time manipulation of the FCDI system with recycled AC slurry. Therefore, it is essential to testify the durability and stability of adsorption towards ammonium by FCDI with 10 % AC_{200} mixed with 1.5 % graphene. As shown in Fig. S5, the recycled electrode further reused to repeat the adsorption test on NH_4^+ within ten-cycle consecutive FCDI manipulation. It reveals that recycled graphene-AC electrode maintains stable NH_4^+ adsorption over ten-cycle tests, with only marginal decreases in NH_4^+ recovery efficiency as low as ~10 %. In summary, graphene-AC electrodes can enhance ammonium recovery by accelerating charge transfer and reduced resistance. Meanwhile, stable NH_4^+ adsorption across repeated FCDI tests proves their durability and feasibility for long-term ammonium recovery. It is worth noting that NH_4^+ adsorption rate is subject to the ratio of graphene and nano-sized AC for FCDI.

3.4. *Electrochemical behavior of graphene-AC electrodes towards NH_4^+ recovery*

Electrochemical performance was tested to assess the influence of graphene and AC content on charge storage and ion adsorption by FCDI. Fig. 6a shows that 10 % AC_{200} mixed with $GP_{1.5}$ electrode exhibits the highest capacitance with the largest quasi-rectangular CV area, indicating enhanced charge storage and electrosorption performance. Graphene can facilitate electron mobility due to its high conductivity, whereas the increase in AC electrodes provides additional ion-accessible sites, reinforcing the charge retention capacity [26,39]. The enhanced interaction between AC and graphene forms a conductive percolation network within carbon-based electrodes and optimize charge mobility to improve electrochemical efficiency [42]. Specific capacitance analysis at 20 mV/s further confirms the role of graphene in enhancing charge transport and ion accessibility, as evidenced by the 2.53-fold increase in capacitance for 10 % AC_{200} + $GP_{1.5}$ compared to 10 % AC_{200} (Fig. 6b). The combined effect of graphene and AC facilitates charge transfer and ion accessibility, thereby enhancing the adsorption process. However, at a lower AC content (7.5 % AC_{200} + $GP_{1.5}$), the impact of graphene remains limited due to insufficient electroactive

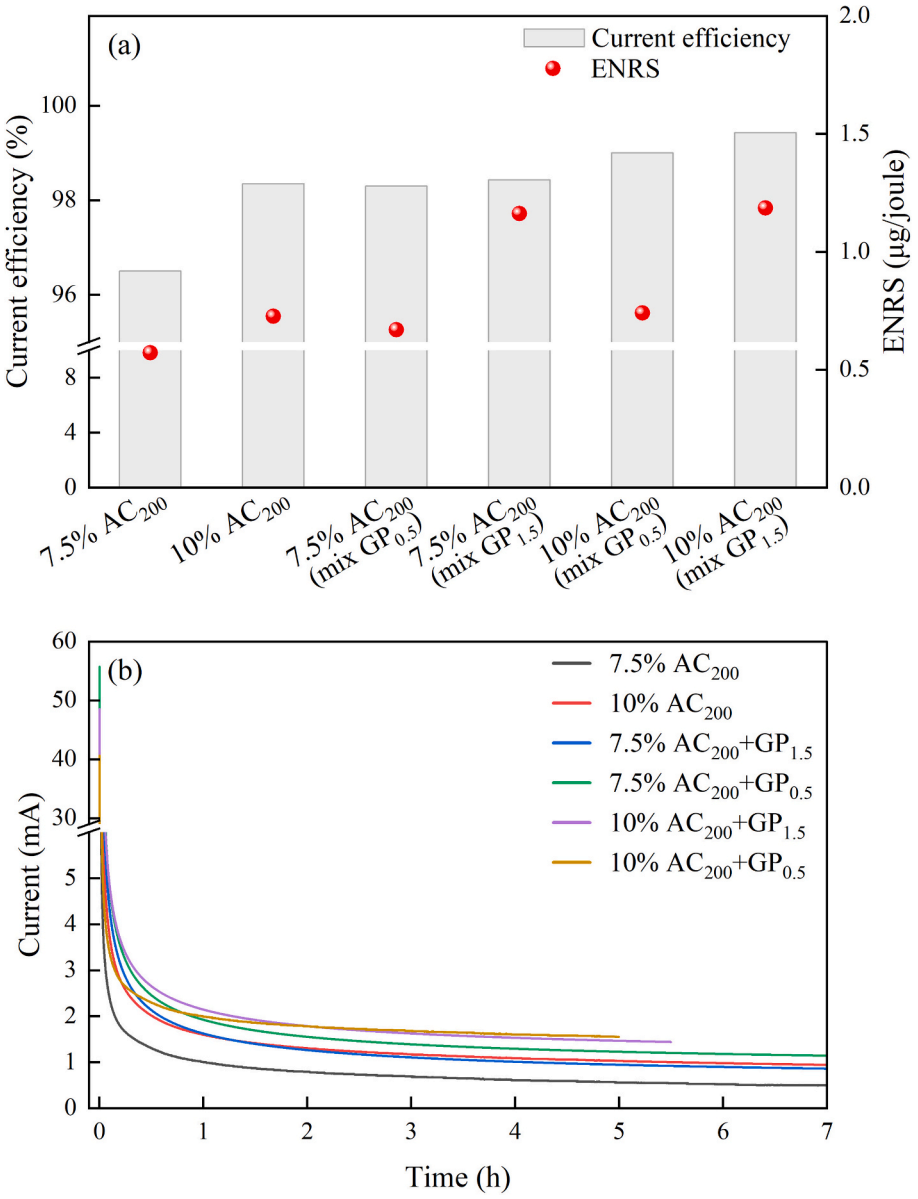

Fig. 7. Variation of (a) charge efficiency and energy-normalized removed salt (ENRS), (b) current at the different $_{AC200}$ (200 nm) contents and the addition of graphene during 7 h of FCDI operation at 1.4 V (initial pH of feed solution: 7 ± 0.2 and operating pH of AC slurry: 8.8 ± 0.2).

surface availability [43]. Based on CV tests, the area of CV cycle indicates that stand-alone AC exhibits low ion storage capacity while the combination of graphene with AC can enhance ion storage. Therefore, it is critical to maintain the ratio of AC and graphene for efficient manipulation of FCDI.

The charge transport mechanism is clarified through EIS analysis (Fig. 6c), which reveals trends in electron transfer resistance and ion diffusion. The increase in AC amount and the addition of graphene reduce the semicircle diameter in the high-frequency region, indicating lower electron transfer resistance between the porous nano-sized AC and the current collector. In that case, a high density of AC percolation network enhances charge transport pathways and reduces slurry resistance [31]. A previous study has revealed that a larger semicircle diameter is generally caused by the inability of ions to enter the pore of AC [44]. In the low-frequency region, the Warburg impedance slopes indicate that higher graphene amount improves ion diffusion across all AC concentrations. The two-dimensional graphene structure reduces diffusion barriers and accelerates ion mobility within graphene-AC mixed electrodes [40]. The absence of redox peaks over multiple scan rates for the 10 % AC_{200} + $GP_{1.5}$ electrode indicates that there is a predominantly EDL adsorption mechanism (Fig. 6d) and no faradaic reaction during ammonium electrosorption [22]. The electrochemical behavior of graphene-AC electrodes suggests that electrochemical performance can be facilitated by the synergistic effect of graphene-AC electrodes in the manipulation of FCDI where graphene improves ion transport and accessibility to lower resistance and enhance electrosorption.

3.5. Specific energy consumption of graphene-AC FCDI for NH_4^+ recovery

The synergistic effects of graphene and AC slurry electrode on energy efficiency and salt removal were further determined following Eqs. 4 and 5, as shown in Fig. 7a. A 7.5 wt% AC electrode without graphene reaches a charge efficiency (CE) of 96.5 % and energy-normalized salt removal (ENRS) of 0.5717 μmol/J, indicating limited charge transport and insignificant ion adsorption. With addition of 0.5 % graphene (AC_{200} + $GP_{0.5}$), it achieves CE of 98.30 % and an ENRS of 0.6695 μmol/J. With increase in the amount of graphene to 1.5 % (AC_{200} + $GP_{1.5}$), it

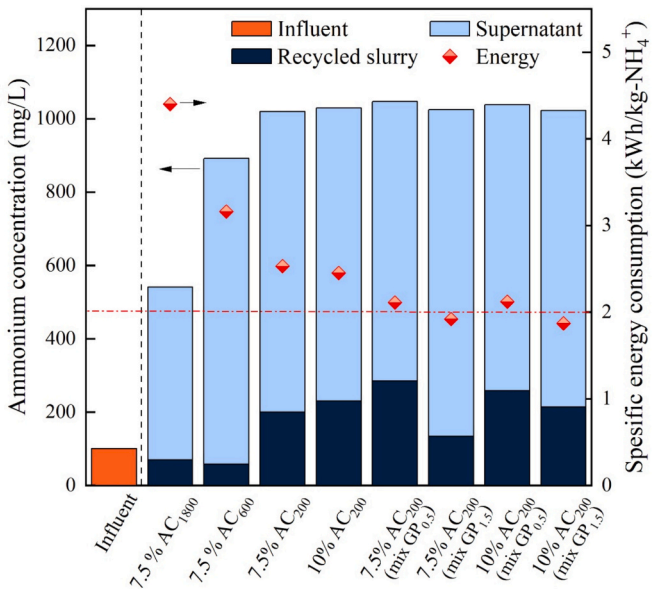

Fig. 8. Variations of energy consumption and ammonium concentration in the influent, supernatant, and recycled electrode from various AC slurries in each FCDI test (Voltage: 1.4 V; initial pH of feed solution: 7 ± 0.2; operating pH of AC slurry: 8.8 ± 0.2).

further increases the CE to 98.43 % and ENRS to 1.1618 μmol/J. These phenomena confirm that graphene facilitates ion charge transport and lowers energy input for NH_4^+ adsorption. An increase in AC content to 10 % (10 % C_{200} + $GP_{0.5}$), it further amplifies efficiency of current and energy input where the highest CE and ENRS at approximately 99 % and 0.7399 μmol/J are observed, respectively. At such a condition, the increase in graphene amount to 1.5 % can reach the highest CE and ENRS, corresponding to 99.43 % and 1.1852 μmol/J, respectively. This improvement on CE and ENRS could be caused by the larger electroactive surface of smaller AC. A previous study has revealed that the larger electroactive by AC can effectively improve the adsorption capacity and promote efficient charge-transfer interactions [31]. However, an excessive amount of AC electrodes is able to rise viscosity of slurry and hinder ion mobility, as previously reported [25]. On the other hand, the stability of the current overtime further echoes the improvements in energy efficiency. FCDI equipped with best ratio of AC and graphene (10 % AC_{200} + $GP_{1.5}$) exhibits minimum current fluctuations, indicating optimized charge retention and ion transport efficiency (Fig. 7b). In contrast, the presence of 7.5 % AC_{200} shows fluctuating current trends, which echoes its limited charge utilization and insignificant ions adsorption. These results suggest that graphene enhances charge mobility by mediating the transfer of electron, while AC stabilizes ion adsorption cycles and reduces resistive losses.

Fig. 8 illustrates the impact of the AC size and graphene addition on ammonium recovery and energy consumption. Reducing the AC diameter from AC_{1800} to AC_{200} can improve ammonium adsorption efficiency. At such a condition, energy consumption significantly reduces from approximately 4.5 to 2.1 kWh/kg-NH_4^+. This phenomenon confirms that smaller AC diameters improve the charge transfer efficiency and ion transport pathways, reducing the resistance and lowering the energy input for ion removal [25,45]. The synergistic effect of graphene addition and increased AC content from 7.5 to 10 wt% facilities higher ammonium adsorption efficiency. By using FCDI with optimized ratio of graphene and AC electrodes (10 % AC_{200} + $GP_{1.5}$), the concentration reaches up to ~1000 mg-NH_4^+/L and the corresponding energy consumption minimizes to 1.87 kWh/kg-NH_4^+. Previous studies have reported that recovery of 20–43 mg/L NH_4Cl using pure AC electrodes (5–15 wt%) required 4.7–35.4 kWh/kg-NH_4^+ [16,17,26]. Whereas carbon-based composite modifications (e.g., KTO, AC-Ni, CB, and $Ti_3C_2T_x$-MXene) reduced energy consumption to 0.45–2.49 kWh/kg-NH_4^+ [19,27,45]. The detailed energy consumption across different FCDI configurations for ammonium recovery are summarized in Table S2. Graphene facilitates charge transfer by improving electron mobility and enhancing electrochemical conductivity. Additionally, the increased AC content provides additional active adsorption sites, optimizing ammonium adsorption and storage. Furthermore, the stable current profiles over extended operational periods further demonstrate the optimized AC-to-graphene ratio to effectively enhance charge utilization.

3.6. *Testification of ammonium recovery from municipal wastewater by graphene-AC FCDI*

The practical applicability of graphene-AC FCDI for energy-efficient ammonium recovery from municipal wastewater was further testified, as shown in Fig. 9. As shown in Fig. 9a, conductivity rapidly decreases within 4 h and reaches the minimum (42 μS/cm from ~1953 μS/cm) after 7 h. Meanwhile, the normalized adsorption ratio of NH_4^+ and co-existing ions declines sharply, with removal efficiency of approximately 75–95 % where it exhibits higher reduction in NH_4^+ and Na^+, as evidenced in Fig. 9b. As reported previously, monovalent ion such as NH_4^+ exhibits preferential electrosorption with ~1.5 to 2.8× higher diffusion coefficient and smaller hydrated radius (NH_4^+ = 3.58 Å) relative to Na^+, Ca^{2+}, and Mg^{2+} which are 3.58, 4.12, and 4.28 Å,

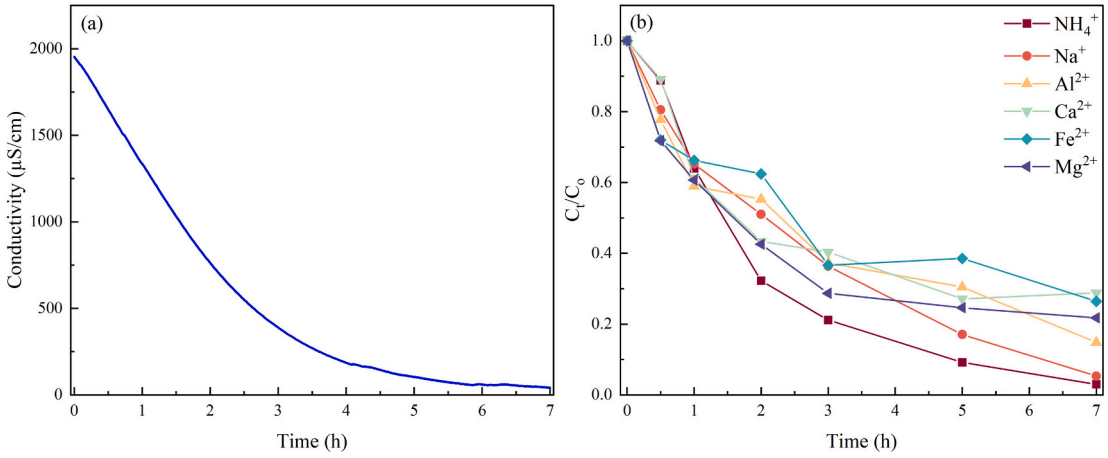

Fig. 9. Changes in (a) conductivity and (b) normalized adsorption ratio of NH_4^+ and co-existing ions of the effluent from municipal WWTP by FCDI with 10 % AC_{200} and 1.5 % graphene (Reaction time: 7 h, voltage: 1.4 V, initial pH of feed solution: 7 ± 0.2, operating pH of AC_{200} slurry: 8.8 ± 0.2, initial concentration of NH_4^+: 5.56 mM; Al^{3+}:0.104 mM; Ca^{2+}:1.25 mM; Fe^{2+}:0.0225 mM; Mg^{2+}:2.00 mM and Na^+:6.22 mM).

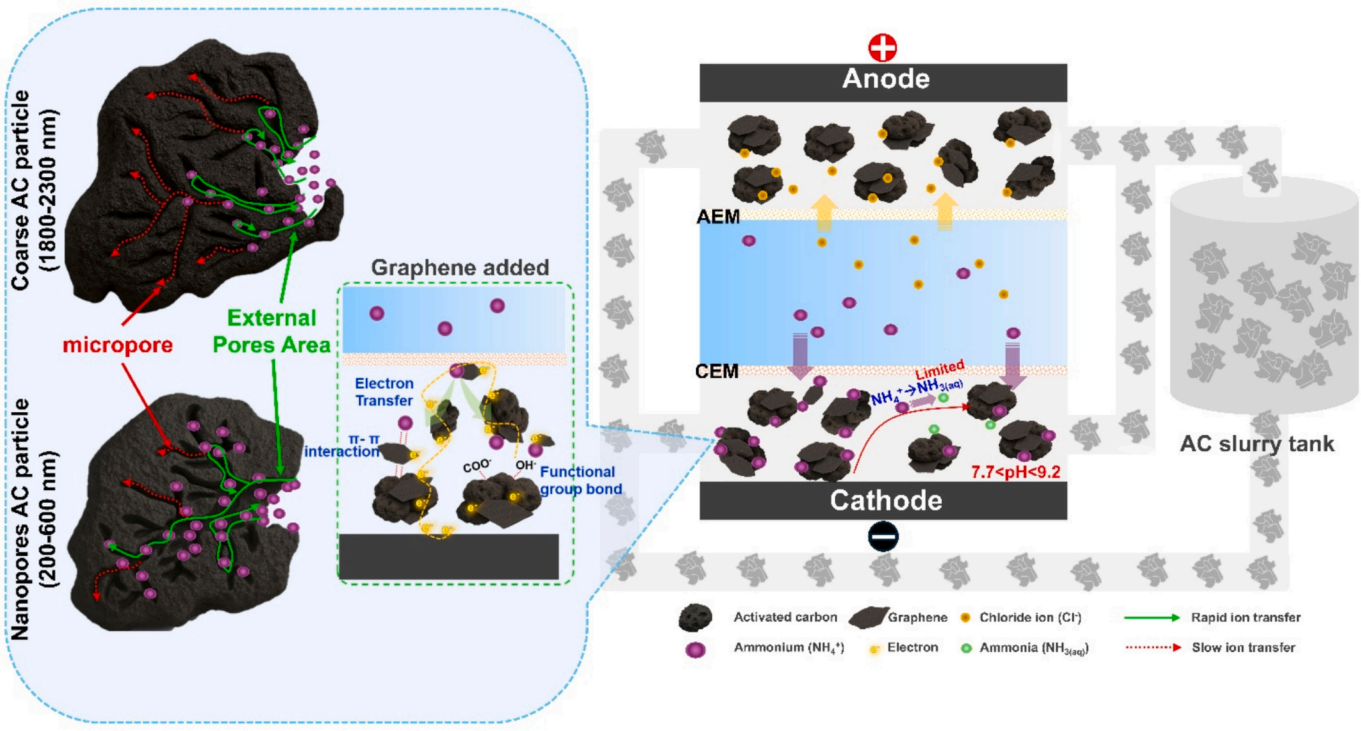

Fig. 10. Proposed mechanisms of ammonium recovery by FCDI using graphene-AC electrodes.

respectively [26,46]. However, the energy input of graphene-AC FCDI reaches at 2.24 kWh/kg-NH_4^+ after 7 h adsorption. Based on the findings of testified study, the graphene-AC_{200} mixture (10 % AC_{200} + $GP_{1.5}$) demonstrates an effective and largely non-selective adsorption towards the existing ions from the effluent of municipal WWTP. This non-selective behavior appears because graphene–AC_{200} mixture provides abundant accessible adsorption sites, enabling rapid ion transport and simultaneous uptake of both monovalent and divalent species. It concludes that energy-efficient NH_4^+ recovery from low-concentration wastewater by FCDI using graphene/ nano-sized AC electrode is feasible for practical applications.

3.7. Mechanistic insight and signature of NH_4^+ recovery by energy-efficient FCDI with graphene-AC

Recovery of ammonium from wastewater by energy-efficient FCDI system can be achieved through electrosorption, charge-assisted migration, and ion diffusion to the carbon matrix [31,47]. In this study, the proposed mechanisms of NH_4^+ ion adsorption by FCDI using graphene-AC electrode is illustrated in Fig. 10. NH_4^+ migrates towards the cathode chamber containing negatively charged AC electrodes. The functional groups (—COO^-, —OH, C═O) on nanopore AC surfaces enhance NH_4^+ adsorption by facilitating electrostatic interactions. In addition, smaller AC electrodes can provide a high flowability and interconnectivity for superior NH_4^+ transfer to AC surface [25]. When the size of AC electrodes reduces to nano dimensions at 600 nm and 200 nm (AC_{600} and AC_{200}) from micro diameter at 1800 nm (AC_{1800}), the nano-sized AC electrodes induce faster NH_4^+ transfer to the surface of AC and then diffuse to larger external pore areas available for NH_4^+ adsorption. For this study, the characterization of AC electrodes at different sizes in the AC-based FCDI has indicated that external ion transfer is dominated by particle size, whereas pore architecture regulates intraparticle diffusion and adsorption into internal pore regions. As a result, the larger external surface area and higher mesopore availability of nano-sized AC (AC_{200} and AC_{600}) dominantly promote rapid NH_4^+ diffusion and adsorption by FCDI, as evidenced in Fig. 2 and Fig. 4. In summary, the use of micro-size AC electrodes does affect external ion transfer and NH_4^+ adsorption aside from pore size effect, while the dominant effect of external pore size on NH_4^+ adsorption occurs in the use of nano-sized AC electrodes regardless of AC diameter (AC_{600} and AC_{200}).

As graphite is added in micro-size AC electrode slurry, it can significantly improve energy input efficiency, as reported previously [26]. In this study, AC_{200} has the lowest specific energy consumption along with highest NH_4^+ adsorption, indicating nano-sized AC electrodes (AC_{600} and AC_{200}) favor more effective interconnectivity between each other along with less power input, as evidenced in Table S3. Theoretically, the addition of sheet-like graphene could further improve charge mobility and reduce charge-transfer resistance mostly in the use of AC_{200} electrodes compared to larger ones. Based on the findings of NH_4^+ recovery capacitance and energy input in the combination of AC and graphene, as indicated in Fig. 8, it has been proven that the proper AC-graphene ratio can minimize the energy input for the maximization of NH_4^+ adsorption by FCDI. Thus, the synergistic effect of nano-sized AC electrodes mixed with graphene at a proper ratio for energy-efficient NH_4^+ recovery is technically feasible in the combination of superior pore adsorption and stronger charge transfer at high percolation network between nano-sized AC electrodes and sheet-like graphene, as illustrated by SEM survey in Fig. S2e. While real wastewater treatment involves challenges such as co-ion competition, fluctuating adsorption, and organic interference, as shown in Fig. 9, this study has established a clear material design strategy by adjusting the ratio of mixed AC and graphene for NH_4^+ recovery. It concludes that the FCDI with AC-graphene is scalable and has potential to reach the energy-efficient recovery of NH_4^+ at cost-effective operation for wastewater treatment.

4. Conclusions

The FCDI system with graphene-AC electrodes demonstrates effective NH_4^+ recovery in high energy efficiency at optimized graphene/ nano-sized AC ratio. The addition of graphene to AC electrode enhances electrical conductivity and facilitates rapid NH_4^+ ion transport. With 1.5 % graphene, increasing the AC_{200} amount to 10 % further

improves NH_4^+ adsorption rate and specific capacitance mostly. At such a condition, more active sites from external surface area are available for stable and efficient NH_4^+ adsorption. The optimal AC-graphene ratio achieves an ammonium concentrating factor exceeding 10× within 5 h (i.e., recycled NH_4^+ concentration is around 1023 mg-NH_4^+/L) and minimizes resistive losses and improves ion transfer, with low energy demand for approximately 1.87 kWh/kg-NH_4^+. In addition, energy-efficient NH_4^+ recovery from low-concentration wastewater by FCDI using graphene/nano-sized AC electrode is feasible for practical applications. It is concluded that the energy-efficient manipulation of FCDI can be achieved by controlling optimized AC-to-graphene ratio of electrodes to concentrate NH_4^+ from the effluent of municipal WWTP.

CRediT authorship contribution statement

Fahrudin Sidik: Writing – original draft, Methodology, Investigation, Formal analysis, Data curation. **Jr-Lin Lin:** Writing – review & editing, Validation, Supervision, Resources, Funding acquisition, Conceptualization. **Ya-Ju Juang:** Resources, Funding acquisition. **Guan-You Lin:** Resources, Funding acquisition.

Declaration of competing interest

The authors declare that they have no known competing financial interests or personal relationships that could have appeared to influence the work reported in this paper.

Acknowledgement

The authors would like to extend their appreciation to the Industrial Technology Research Institute, Taiwan for assistance in financial support.

Appendix A. Supplementary data

Supplementary data to this article can be found online at https://doi.org/10.1016/j.seppur.2025.136477.

Data availability

The authors do not have permission to share data.

References

[1] L. He, Y. Wang, T. Zhou, Y. Zhao, Enhanced ammonia resource recovery from wastewater using a novel flat sheet gas-permeable membrane, Chem. Eng. J. 400 (2020) 125338.
[2] B. Tang, K. Jiang, W. Yin, W. Xing, J. Zhang, S. Pi, J. Liang, L. Tang, W. Tang, Coupling of nitrate electroreduction to ammonia with sulfide electrooxidation to sulfur for high-efficiency wastewater treatment and resource recovery, Small 21 (2025) e08173.
[3] D. Yang, H. Liu, Q. She, Mixed cation transport behaviours in electrodialysis during simultaneous ammonium enrichment and wastewater desalination, Desalination 545 (2023) 116155.
[4] W. Fan, Y. Wang, R. Liu, J. Zou, X. Yu, Y. Liu, C. Zhi, J. Meng, Textile production by additive manufacturing and textile waste recycling: a review, Environ. Chem. Lett. 22 (2024) 1929–1987.
[5] A.K. Saim, Ammoniacal leaching for the extraction of valuable metals from secondary resources: a review, Miner. Process. Extr. Metall. Rev. (2024) 1–22.
[6] V. Innocenzi, S.B. Zueva, N.M. Ippolito, F. Ferella, M. Prisciandaro, F. Vegliò, A review of the existing and emerging technologies for wastewaters containing tetramethyl ammonium hydroxide (TMAH) and waste management systems in micro-chip microelectronic industries, Chemosphere 307 (2022) 135913.
[7] S. Fukumoto, T. Matsumae, Y. Kurashima, H. Takagi, H. Umezawa, M. Hayase, E. Higurashi, Heterogeneous direct bonding of diamond and semiconductor substrates using NH3/H2O2 cleaning, Appl. Phys. Lett. 117 (2020).
[8] A. Gordano, Chapter one - composite membrane based systems, in: A. Basile, M. R. Rahimpour (Eds.), Progresses in Ammonia: Science, Technology and Membranes, Elsevier, 2024, pp. 1–46.
[9] W.A.F. Wae AbdulKadir, R. Che Omar, M.H.Z. Mohd Harun, A.L. Ahmad, Innovative two-stage membrane distillation: a breakthrough in ammonia removal and recovery, Desalination 615 (2025) 119225.
[10] B. Maqdasi, E. Alhseinat, J. Rodríguez, K. Al-Ali, Ammonia recovery from wastewater: a critical review of technologies with emphasis on capacitive deionization, Chem. En. J. Adv. 24 (2025) 100901.
[11] D. Fang, X. Song, B. Liu, F. Li, P. Zhang, C. Li, X. Mo, K. Li, A novel sustainable N recycling process: upcycling ammonia to ammonium fertilizer from dilute wastewater and simultaneously realizing phenol degradation via a visible solar-driven PECMA system with efficient Ag2S-BiVO4 photoanodes, Sci. Total Environ. 864 (2023) 161121.
[12] H. Sakar, I. Celik, C. Balcik-Canbolat, B. Keskinler, A. Karagunduz, Ammonium removal and recovery from real digestate wastewater by a modified operational method of membrane capacitive deionization unit, J. Clean. Prod. 215 (2019) 1415–1423.
[13] Z. Ge, X. Chen, X. Huang, Z.J. Ren, Capacitive deionization for nutrient recovery from wastewater with disinfection capability, Environ. Sci.: Water Res. Technol. 4 (2018) 33–39.
[14] M. Askari, S. Rajabzadeh, L. Tijing, H.K. Shon, Advances in capacitive deionization (CDI) systems for nutrient recovery from wastewater: paving the path towards a circular economy, Desalination 583 (2024) 117695.
[15] Y. Yang, B. Tao, C. Liu, M. Li, W. Wu, Y. She, J. Zhang, H.K. Thabet, M.H. Helal, Z. M. El-Bahy, X. Xu, Capacitive deionization for ammonia recovery: progresses and challenges, Chem. Eng. J. 500 (2024) 157324.
[16] K. Fang, W. He, F. Peng, K. Wang, Ammonia recovery from concentrated solution by designing novel stacked FCDI cell, Sep. Purif. Technol. 250 (2020) 117066.
[17] C. Zhang, J. Ma, J. Song, C. He, T.D. Waite, Continuous Ammonia recovery from wastewaters using an integrated capacitive flow electrode membrane stripping system, Environ. Sci. Technol. 52 (2018) 14275–14285.
[18] C. Li, B. Liu, D. Fang, P. Zhang, F. Li, X. Qiu, X. Mo, K. Li, Polyaniline-derived mesoporous carbon electrode for selective and efficient ammonium removal with in a flow-electrode capacitive deionization system, J. Environ. Chem. Eng. 11 (2023) 110857.
[19] L. Lin, J. Hu, J. Liu, X. He, B. Li, X.-Y. Li, Selective ammonium removal from synthetic wastewater by flow-electrode capacitive deionization using a novel $K_2Ti_2O_5$-activated carbon mixture electrode, Environ. Sci. Technol. 54 (2020) 12723–12731.
[20] C. Zhang, J. Ma, L. Wu, J. Sun, L. Wang, T. Li, T.D. Waite, Flow electrode capacitive deionization (FCDI): recent developments, environmental applications, and future perspectives, Environ. Sci. Technol. 55 (2021) 4243–4267.
[21] T. Chen, L. Xu, S. Wei, Z. Fan, R. Qian, X. Ren, G. Zhou, H. Yang, J. Wu, H. Chen, Ammonia-rich solution production from coal gasification gray water using chemical-free flow-electrode capacitive deionization coupled with a monovalent cation exchange membrane, Chem. Eng. J. 433 (2022) 133780.
[22] Y. Qu, Y. Pan, L. Wu, H. Zhu, Mitigation of salinity buildup in hybrid flow-electrode capacitive deionization-osmotic membrane bioreactor for sludge anaerobic digestion, Chem. Eng. J. 435 (2022) 134885.
[23] C. Hou, S. Peng, Z. Zhou, L. Xu, Y. Wang, J. Zhu, P. Zhang, Z. Chen, Z. Lei, D. Wu, Selective ammonia recovery from wastewater by SDS-AC based microfiltration membrane flow electrode capacitor deionization, Sep. Purif. Technol. 359 (2025) 130555.
[24] H.M. Saif, B. Ferrández-Gómez, V.D. Alves, R.M. Huertas, G. Alemany-Molina, A. Viegas, E. Morallón, D. Cazorla-Amorós, J.G. Crespo, S. Pawlowski, Activated carbons for flow electrode capacitive deionization (FCDI) – morphological, electrochemical and rheological analysis, Desalination 602 (2025) 118638.
[25] M. Tauk, M. Bechelany, S. Lagerge, P. Sistat, R. Habchi, M. Cretin, F. Zaviska, Influence of particle size distribution on carbon-based flowable electrode viscosity and desalination efficiency in flow electrode capacitive deionization, Sep. Purif. Technol. 306 (2023) 122666.
[26] K. Fang, H. Gong, W. He, F. Peng, C. He, K. Wang, Recovering ammonia from municipal wastewater by flow-electrode capacitive deionization, Chem. Eng. J. 348 (2018) 301–309.
[27] N.E. Mansoor, L.A. Diaz, C.E. Shuck, Y. Gogotsi, T.E. Lister, D. Estrada, Removal and recovery of ammonia from simulated wastewater using Ti3C2Tx MXene in flow electrode capacitive deionization, npj Clean Water 5 (2022) 26.
[28] P. Liang, X. Sun, Y. Bian, H. Zhang, X. Yang, Y. Jiang, P. Liu, X. Huang, Optimized desalination performance of high voltage flow-electrode capacitive deionization by adding carbon black in flow-electrode, Desalination 420 (2017) 63–69.
[29] S. Mani, B. Thangapandi, P. Elangovan, A. Prakash, R. Subbaiah, S. Vasudevan, M. Rajendran, New insights into the performance analysis of flow-electrode capacitive deionization using ferri/ferrocyanide redox couples for continuous water desalination, Chem. Eng. J. 480 (2024) 147887.
[30] H. Jiang, J. Zhang, K. Luo, W. Xing, J. Du, Y. Dong, X. Li, W. Tang, Effective fluoride removal from brackish groundwaters by flow-electrode capacitive deionization (FCDI) under a continuous-flow mode, Sci. Total Environ. 804 (2022) 150166.
[31] T. Wang, Z. Zhang, Z. Gu, C. Hu, J. Qu, Electron transfer of activated carbon to anode excites and regulates desalination in flow electrode capacitive deionization, Environ. Sci. Technol. 57 (2023) 2566–2574.
[32] Z. Sumaraj, A.K. Xiong, L.P. Sarmah, Padhye, acidic surface functional groups control chemisorption of ammonium onto carbon materials in aqueous media, Sci. Total Environ. 698 (2020) 134193.
[33] G. Folaranmi, M. Tauk, M. Bechelany, P. Sistat, M. Cretin, F. Zaviska, Investigation of fine activated carbon as a viable flow electrode in capacitive deionization, Desalination 525 (2022) 115500.
[34] L. Liu, Y. Ahmadi, K.-H. Kim, D. Kukkar, J.E. Szulejko, The relative dominance of surface oxygen content over pore properties in controlling adsorption and retrograde behavior of gaseous toluene over microporous carbon, Sci. Total Environ. 906 (2024) 167308.

[35] J. Qu, J. Liu, N.A. Al-Dhabi, Y. Leng, J. Yi, K. Jiang, W. Xing, D. Yin, W. Tang, Ni-EDTA decomplexation and Ni removal from wastewater by electrooxidation coupled with electrocoagulation: optimization, mechanism and biotoxicity assessment, Sep. Purif. Technol. 376 (2025) 133980.
[36] A. Awasthi, K. Gandhi, S. Rayalu, Carbon nanomaterials for facilitated solar-powered wastewater treatment, Mater. Today Proc. 77 (2023) 300–306.
[37] D. Dittmann, L. Saal, F. Zietzschmann, M. Mai, K. Altmann, D. Al-Sabbagh, P. Schumann, A.S. Ruhl, M. Jekel, U. Braun, Characterization of activated carbons for water treatment using TGA-FTIR for analysis of oxygen-containing functional groups, Appl Water Sci 12 (2022) 203.
[38] B.M. Thamer, F.A. Al-aizari, H.S. Abdo, A.M. Al-Enizi, Activated carbon-decorated electrospun polystyrene fibers for highly efficient removal of hazardous crystal violet dye from water, Colloids Surf. A Physicochem. Eng. Asp. 688 (2024) 133612.
[39] L. Chang, Y. Fei, Y.H. Hu, Structurally and chemically engineered graphene for capacitive deionization, J. Mater. Chem. A 9 (2021) 1429–1455.
[40] K. Tang, S. Yiacoumi, Y. Li, C. Tsouris, Enhanced water desalination by increasing the electroconductivity of carbon powders for high-performance flow-electrode capacitive deionization, ACS Sustain. Chem. Eng. 7 (2018) 1085–1094.
[41] P. Liu, T. Yan, L. Shi, H.S. Park, X. Chen, Z. Zhao, D. Zhang, Graphene-based materials for capacitive deionization, J. Mater. Chem. A 5 (2017) 13907–13943.
[42] Z. Zhu, J. Xiong, M. Chen, L. Mu, X. Lu, J. Zhu, Insights into the particle hydrophilicity and electrical conductivity for the construction of a highly efficient electrical percolation network in flow electrode capacitive deionization, Ind. Eng. Chem. Res. 62 (2023) 17721–17730.
[43] S. Gupta, C. Price, Investigating graphene/conducting polymer hybrid layered composites as pseudocapacitors: interplay of heterogeneous electron transfer, electric double layers and mechanical stability, Compos. Part B Eng. 105 (2016) 46–59.
[44] H. El Ouahabi, A. Elmouwahidi, L. Cano-Casanova, M.Á. Lillo-Ródenas, M. C. Roman-Martínez, A.F. Pérez-Cadenas, E. Bailón-García, M. Shaban, G.M. Al-Senani, M. Ouzzine, M. Khaddor, From nutshells to energy cells: pioneering supercapacitor electrodes via innovative argan nutshell activated carbon synthesis, J. Energy Storage 82 (2024) 110598.
[45] T. Chen, L. Xu, S. Wei, X. Tang, H. Chen, Enhanced ammonia-rich solution production and electrode separation using magnetic nickel-loaded carbon black in flow-electrode electrochemical deionization (FEED), Desalination 544 (2022) 116152.
[46] Y. Li, C. Zhang, Y. Jiang, T.-J. Wang, H. Wang, Effects of the hydration ratio on the electrosorption selectivity of ions during capacitive deionization, Desalination 399 (2016) 171–177.
[47] T. Sun, B.D.A. Levin, J.J.L. Guzman, A. Enders, D.A. Muller, L.T. Angenent, J. Lehmann, Rapid electron transfer by the carbon matrix in natural pyrogenic carbon, Nat. Commun. 8 (2017) 14873.